View metadata, citation and similar papers at core.ac.uk

brought to you by CORE

provided by Elsevier - Publisher Connector

International Journal of Heat and Mass Transfer 104 (2017) 1083–1089

Contents lists available at ScienceDirect

International Journal of Heat and Mass Transfer

journal homepage: www.elsevier.com/locate/ijhmt

Optimization of wick shape in a loop heat pipe for high heat transfer

M. Nishikawara [a,*], H. Nagano [b]

[a] Department of Mechanical Engineering, Toyohashi University of Technology, 1-1, Hibarigaoka, Tempaku, Toyohashi, Aichi 441-8580, Japan
[b] Department of Mechanical Science and Engineering, Nagoya University, Furo, Chikusa, Nagoya 464-8603, Japan

ARTICLE INFO

Article history:
Received 8 August 2016
Accepted 10 September 2016
Available online 17 September 2016

Keywords:
Capillary evaporator
Capillary pumped loops
Evaporator heat-transfer coefficient
Loop heat pipe
Optimized wick shape
Three-phase contact line

ABSTRACT

This paper presents a method to optimize wick shape in the capillary evaporator of loop heat pipes and capillary pumped loops. The evaporator heat-transfer coefficient is maximized using only the length of a three-phase contact line (TPCL) within the case, wick, and grooves as a variable wick dimension. The heat-transfer coefficient is formulated taking the following two particular aspects into account. The heat-transfer coefficient initially increases with TPCL length. However, when TPCL becomes too long, the heat-transfer coefficient decreases because of a large pressure loss in the grooves. The proposed model is validated experimentally. Both the model and experiment show the heat-transfer coefficient reached a local maximum in terms of the TPCL length. It is concluded that wick shape can be optimized by just using the TPCL length. The effects of the material of an evaporator's case, wick, and working fluid are also discussed.

© 2016 The Authors. Published by Elsevier Ltd. This is an open access article under the CC BY-NC-ND license (http://creativecommons.org/licenses/by-nc-nd/4.0/).

1. Introduction

Loop heat pipes (LHPs) and capillary pumped loops (CPLs) are high-capacity passive heat-transport devices that are powered by capillary pressure in a porous medium and evaporation/condensation of a working fluid. Unlike conventional heat pipes, the porous medium (wick) is solely located in the evaporator; this facilitates longer transport lengths and larger radiation areas. The two devices are used widely in various thermal-control applications, such as in spacecrafts [1], printed circuit boards [2], insulated-gate bipolar transistors (IGBTs) [3], thermoelectric generators [4], solar water heaters [5], laptops [6], and light-emitting diodes (LEDs) [7]. A schematic of an LHP is shown in Fig. 1. It comprises a capillary evaporator, condenser, transport line, and compensation chamber (CC). The condenser and transport line are simple pipes. The evaporator configuration is the critical part of the performance design. However, an optimal method for designing this component is yet to be established.

Previous studies have tended to adopt one of the following two approaches for enhancing the evaporator performance, i.e., the heat-transfer coefficient and maximum heat transfer. The first approach is to use various porous materials and capillary structures [8–11]. Some studies have shown that using biporous or two-layer wicks can increase the evaporator heat-transfer coefficient [8–10]. Kiseev et al. maximized the heat-transport rate by optimizing the pore size of the wick [11]. The second approach involves changing the shape of the wick and grooves [12–25]. This paper adopts the second approach with an aim to optimize the classical wick shape of an inverted meniscus, across which heat and fluid flow in opposite directions. Excluded from this paper are the noninverted meniscus [12], across which the two flows are in the same direction, and the approach of maintaining a gap between the wick and its case [13,14]. Previous parametric studies that have attempted to enhance evaporator performance are listed in Table 1. For each study, the evaporator shape and the variables that were changed are listed.

North et al. [15] adopted two approaches using a cylindrical evaporator that comprised a 304 stainless steel (SS) case and ammonia as the working fluid. The first approach was to increase the number and to decrease the size of the circumferential grooves. The second approach was to fill the circumferential grooves with a biporous material. Both approaches resulted in a heat flux of 0.7 MW/m^2, which was much higher than the limit of 0.07 MW/m^2 when using a classical evaporator at that time, 1997.

Riehl et al. [16] cut 1500 circumferential microgrooves/m in the 316 SS case of a cylindrical evaporator and used an ultra-high-molecular-weight (UHMW) wick and acetone as the working fluid. They also conducted experimental and numerical investigations for another evaporator with 2500 microgrooves/m. The heat-transfer coefficient of the latter evaporator was 60% higher than that of the former. Via a sensitive analysis of the simulation, they showed that this improvement was due to (a) the contact area

* Corresponding author.
E-mail address: nishikawara@me.tut.ac.jp (M. Nishikawara).

http://dx.doi.org/10.1016/j.ijheatmasstransfer.2016.09.027
0017-9310/© 2016 The Authors. Published by Elsevier Ltd.
This is an open access article under the CC BY-NC-ND license (http://creativecommons.org/licenses/by-nc-nd/4.0/).

Nomenclature

A	area (m^2)
d_h	hydraulic diameter (m)
dT/dP_{sat}	gradient of saturation curve (K/Pa)
ΔP	pressure difference (Pa)
ΔT	temperature difference (K)
h_{evap}	evaporator heat-transfer coefficient ($W/m^2 \cdot K$)
h_{sat}	local evaporator heat-transfer coefficient ($W/m^2 \cdot K$)
h_{tri}	contribution for heat transport at the three-phase contact line (W/m·K)
H_{fg}	latent heat (J/kg)
l	length (m)
L_{tri}	length of the three-phase contact line per unit area (/m)
L_z	wick length (m)
$\dot{m}$	mass flow flux ($kg/m^2 \cdot s$)
P	pressure (Pa)
$\dot{q}$	heat flux (W/m^2)
$\dot{q}_{apply}$	heat flux applied to the case (W/m^2)
R	gas constant (J/kg·K)
T	temperature (°C)
T_e	evaporator temperature (°C)
u	velocity (m/s)
z	position for axial direction (m)

Greek

α_c	accommodation coefficient
λ	frictional coefficient
ρ	density (kg/m^3)

Subscripts

ax	axial
ci	circumferential
e	evaporation
evap	evaporator
gr	groove
sat	saturation

between the primary wick and the evaporator housing, (b) wall effectiveness (increase in microgroove density), and (c) total area of the saturated liquid in the microgrooves. However, they did not attempt to further increase the groove density.

Kiseev et al. [17] conducted parametric experiments in which they changed the wick material, capillary structure, wick thickness, cross-sectional groove shape (rectangular, trapezoidal, or triangular), groove layout (i.e., number density), groove location (i.e., in the case or wick), and working fluid (water, acetone, or ammonia). They used a flat disk-shaped evaporator for copper. Their extensive experiments proved to be a useful reference. The evaporator heat-transfer coefficient was correlated with the ratio of the total sectional area of the concentric vapor grooves (area of the heater block that is not in contact with the wick) to the area of the heat input (total area of the heater block) and with the hydraulic diameter of the grooves. It was concluded that the optimum area ratio is 0.4–0.5, evaporator efficiency is higher when grooves are placed in the case rather than the wick, and heat-transfer coefficient increases as the grooves become smaller and come closer to each other.

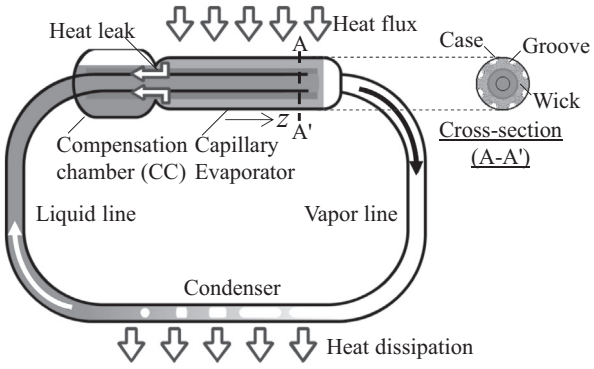

Fig. 1. Loop heat pipe with a classical capillary evaporator.

Kuroi et al. [18] used a cylindrical evaporator in a 304 SS case, a polytetrafluoroethylene (PTFE) wick, and ethanol. They investigated the effects of the number of axial grooves, groove width, contact-area ratio between the case and the wick, and whether or not circumferential grooves were added. The cross-sectional area and depth of each groove were kept constant. It was shown that the evaporator temperature was the lowest with eight grooves. It should be noted that a better performance was achieved using an eight-groove wick than with the 20-groove wick (maximum number of grooves).

Hodot et al. [19] investigated the effect of axial groove number, saddle cross-section shape (connection from the heat source to evaporator), and groove location (case or wick) by performing three-dimensional (3D) simulations of a cylindrical evaporator that comprised a copper case, a nickel wick, and methanol. They showed that the thermal resistance was the lowest for a saddle with a trapezoidal cross-section and for the presence of the most number of grooves and was lower for grooves located in the wick.

Yakomaskin et al. [20,21] used the deformational cutting method (DCM) to create microgrooves in the copper case of a flat, open evaporator, which was not part of a closed loop and comprised a glass-fiber wick (filter paper and SS powder) and

Table 1
Previous research on enhancing the thermal efficiency of evaporators.

Reference	Evaporator shape	Variables affecting evaporator performance
North et al. [15]	Cylinder	Circumferential groove number in the wick and circumferential groove size in the wick
Riehl et al. [16]	Cylinder	Circumferential groove number in the case and circumferential groove number in the wick
Kiseev et al. [17]	Flat (disk)	Wick material, capillary structure, wick thickness, cross-sectional shape of the groove (rectangular, trapezoidal, triangular), groove layout, and groove location (in the wick or case)
Kuroi et al. [18]	Cylinder	Axial groove number (1, 2, 4, 8, 20), groove width, contact area ratio, and circumferential groove added or not
Hodot et al. [19]	Cylinder	Axial groove number (9, 12, 18, 27), saddle shape (flat or trapezoidal), and groove location (in the wick or case)
Yakomaskin et al. [20,21]	Flat (rectangle)	Axial groove number, axial groove width, wick material, capillary structure, and wick thickness
Wu et al. [22]	Cylinder	Axial groove number (8, 10, 12, 14, 16)
Uchida [23]	Flat (rectangle)	Axial groove number

water. Fine grooves with widths of 0.1 mm and 0.3 mm were created. The 0.1-mm-wide groove showed a better performance at low heat fluxes whereas the 0.3-mm-wide groove showed a better performance for higher ones. In the LHP tests, they achieved a heat-transfer coefficient of 12,500 W/m^2 K at 10 W/cm^2 using the 0.1-mm-widegoove, water, and a glass-fiber wick.

Wu et al. [22] conducted experiments in which they changed the number of grooves in a cylindrical evaporator comprising an SS case, a nickel wick, and ammonia. Although their lowest reported thermal resistance was with 14 grooves, this happened to be the maximum number that could be accommodated in the manufacturing process. They proposed a logarithmic relationship between the evaporative surface area (wick surface area) and the maximum heat transport.

Uchida [23] used a copper case with cylindrical pins and a PTFE wick containing holes with the same diameter as the pins to increase the evaporation area in a flat evaporator that used ethanol as the working fluid. Grooves with a width of 0.5 mm were machined on the surface of each hole in the wick. The evaporation area increased to more than double of the original area because of this characteristic shape. The optimum number of pins and the hole diameter in relation to the heat-transfer coefficient were determined via 3D simulations.

Although investigations such as the ones described above have been conducted to enhance evaporator performance, too many variables are involved, e.g., contact surface area, groove width, number of grooves, and groove pitch. Establishing a universal optimization for wick shape is extremely difficult. The addition of circumferential grooves has been shown to lead to a higher heat-transfer coefficient, but the design method in that case is more complicated. A comprehensive and simple approach is needed to optimize wick shape so that the full benefit of circumferential and microgrooves is realized.

In our previous work [26,27], a 3D numerical model was developed to simulate the heat and mass transfers in a capillary evaporator. A pore network model (PNM) was applied to the capillary structure. The fully saturated (i.e., all liquid) and unsaturated (i.e., liquid/vapor) wick states were taken into account. The temperature and pressure in the groove were kept constant. For both states, it was found that the applied heat flux became concentrated at the three-phase contact line (TPCL) within the case, wick, and grooves and then the heat was transferred to the grooves by evaporation. The evaporator heat-transfer coefficient increased when the TPCL was extended by increasing the number of circumferential and axial grooves [27]. This means that the amount of heat transfer at the TPCL is dominant in evaporator heat transfer. Note that the important variable is the length of the TPCL at which the heat flux concentrates and not the contact surface area between the wick and the case. However, for wick shapes whose TPCL is extended, the pressure loss in the groove is considered to have a negative effect because of the much smaller groove size. To the best of our knowledge, thus far, no study has investigated the effects of pressure loss on the evaporator heat-transfer coefficient. Therefore, in this study, a model is formulated in which the effect of pressure loss in the groove on the evaporator heat-transfer coefficient is considered. This leads to the possibility of achieving an optimum wick shape by just using TPCL. The calculated results are validated experimentally.

2. Design of wick shape

The concept for the design of wick shape is as follows. The evaporator heat-transfer coefficient increases with the TPCL length. However, the pressure loss in the grooves increases at the same time, thereby leading to a large distribution of saturation temperature. Consequently, the evaporator heat-transfer coefficient decreases if the TPCL is too long. Because of these competing effects, there is a local maximum in the heat-transfer coefficient at a certain TPCL length, and it is the model of this relationship that is described here. Note that the proposed design method is for the evaporator heat-transfer coefficient and not for enhancing the maximum heat transport (i.e., the capillary limit). The main assumptions of the model are that (1) the fluid is incompressible, (2) the process is a steady-state one, and (3) each groove is filled with saturated vapor.

2.1. Formulation of the evaporator heat-transfer coefficient

The evaporator heat-transfer coefficient h_{evap} is calculated by

$$h_{evap} = \frac{\dot{q}_{apply}}{(T_e - T_{gr})}, \tag{1}$$

where T_e is the temperature of the evaporator case, and T_{gr} is the vapor temperature at the groove outlet to the vapor line.

The fully saturated wick state is considered first. Because the evaporation surface is fixed on the interface between the wick and the groove, the heat-transfer coefficient is dominated by thermal conduction (i.e., thermal conductivity and the effective length and cross-sectional area of the heat-flow path). Convective flow in the wick can normally be neglected. The temperature difference is the one between the temperature of the evaporator case and the saturation temperature in a groove. The saturation temperature varies in the axial direction in a cylindrical evaporator. In any cross-section, the heat flux from the evaporator case to a groove is given by Eq. (2). Even when the wick is in its unsaturated sate, Eq. (2) can be applied to obtain approximate results because the liquid–vapor interface is almost attached to the heating surface near the TPCL and the heat flux there is dominant in the evaporator heat transport. Eq. (2) is written as follows:

$$\dot{q}(z) = h_{sat}(T_e - T_{sat}(z)), \tag{2}$$

where h_{sat} is determined by the thermal conductivity of the wick and the effective length and cross-sectional area over which the heat flows to the evaporation surface and z is the axial direction in the cylindrical evaporator. Because the heat flux concentrates at the TPCL within the case, wick, and grooves, h_{sat} can be considered as the heat-transfer coefficient per unit TPCL length. The saturation temperature in the groove is expressed as a function of pressure:

$$h_{sat} = h_{tri}L_{tri}, \tag{3}$$

$$T_{sat}(z) = T_{sat}[P(z)], \tag{4}$$

where h_{tri} is the contribution of heat transport at the TPCL in W/m·K and L_{tri} is the length of the TPCL in /m. Here, the ratio of $\dot{q}(z)$ to $\dot{q}(Lz)$ is given as:

$$\frac{\dot{q}(z)}{\dot{q}(Lz)} = \frac{h_{sat}(T_e - T_{sat}(z))}{h_{sat}(T_e - T_{sat}(Lz))} = 1 - \frac{T_{sat}(z) - T_{sat}(Lz)}{T_e - T_{sat}(Lz)} = 1 - \frac{dT/dP_{sat}\Delta P_{z-Lz}}{T_e - T_{sat}(Lz)}, \tag{5}$$

in which the relationship between saturation temperature and pressure is

$$\Delta T_{sat} = (dT/dP)_{sat}\Delta P_{sat}. \tag{6}$$

The total heat flux transported by evaporation is

$$\dot{q}_{evap} = \frac{1}{A}\int_0^{Lz} \dot{q}(z)dA = \dot{q}(Lz)\left[1 - \frac{dT/dP_{sat}}{T_e - T_{sat}(Lz)}\frac{1}{A}\int_0^{Lz}\Delta P_{z-Lz}dA\right] \tag{7}$$

where the approximation $\dot{q}_{apply} \approx \dot{q}_{evap}$ is applied. By substituting (7) into (1),

$$h_{evap} = \frac{\dot{q}(Lz)}{T_e - T_{sat}(Lz)}\left[1 - \frac{dT/dP_{sat}}{T_e - T_{sat}(Lz)}\frac{1}{A}\int_0^{Lz}\Delta P_{z-Lz}dA\right] = h_{sat}\left[1 - \frac{dT/dP_{sat}}{T_e - T_{sat}(Lz)}\frac{1}{A}\int_0^{Lz}\Delta P_{z-Lz}dA\right] \quad (8)$$

Here, $T_{gr} = T_{sat}(Lz)$. Finally,

$$h_{evap} = h_{tri}L_{tri}\left[1 - \frac{dT/dP_{sat}}{T_e - T_{sat}(Lz)}\frac{1}{A}\int_0^{Lz}\Delta P_{z-Lz}dA\right] \quad (9)$$

is obtained. The term $h_{tri}L_{tri}$ represents the heat transfer at the TPCL. The right-hand bracket represents the effect of the distribution of saturation temperature in a groove (always <1). The integral term is the pressure loss ΔP_{gr} in a groove, which is the sum of the pressure losses in the axial and circumferential grooves and the pressure loss due to evaporation. Note that ΔP_{gr} can be expressed as:

$$\Delta P_{gr} = \Delta P_{ax} + \Delta P_{ci} + \Delta P_e \quad (10)$$

Terms ΔP_{ax} and ΔP_{ci} are calculated by assuming Poiseuille flow in a circular pipe as follows:

$$\Delta P_{ax} = \lambda\frac{l}{d_h}\frac{1}{2}\rho u^2\frac{1}{2}, \quad (11)$$

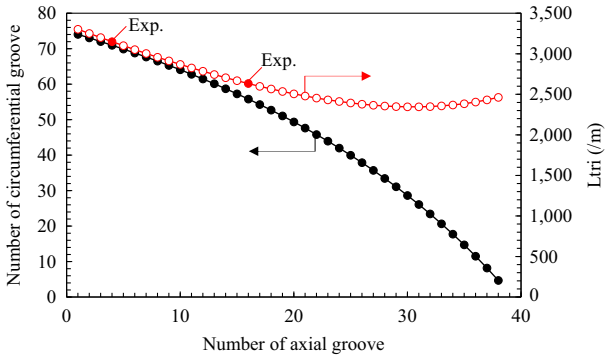

Fig. 2. Variation in the number of circumferential grooves and TPCL length according to the number of axial grooves.

where u is the velocity at the groove outlet. The factor of 1/2 is because of the flow-rate distribution under uniform evaporation. In practical situations, the flow in a groove can differ from Poiseuille flow because of blowing from the wick; nevertheless, ideal flow is assumed in this model. To obtain a detailed pressure distribution in a groove, the Navier–Stokes equations need to be solved in three dimensions. Pressure loss by evaporation [28] is calculated by

$$\Delta P_e = \frac{\sqrt{2\pi RT}\dot{m}}{\alpha_c\left\{1 - \frac{(RT/H_{fg})}{2}\right\}}, \quad (12)$$

where $\alpha_c = 1$ in this model.

2.2. Groove dimension and length of the three-phase contact line

To extend the TPCL, the grooves are made narrower and their number is increased. Clearly, the minimum width of a manufactured groove is limited. In our cylindrical wick, the minimum machined widths are 0.3 mm for a circumferential groove and 0.4 mm for an axial one. Under these limitations, the TPCL length is calculated by changing the numbers of both types of grooves. The ratio of the wick-case contact surface to the cross-sectional area of the case is fixed at 0.5. The cross-sectional area of liquid flow in the wick is therefore the same for all wick shapes, as is the flow resistance in the wick. The maximum heat-transport rate because of the capillary limit also remains the same and is therefore excluded from the discussion. By fixing the area of the wick-case contact surface, the numbers of the circumferential and axial grooves are determined uniquely. The number of circumferential grooves and the length of the TPCL, L_{tri}, are shown in Fig. 2 as functions of the number of axial grooves. Note that L_{tri} is represented as the area density of the heat-load area; therefore, the unit is m^{-1}. Two wicks were manufactured for the experiment: one with four axial grooves, 71 circumferential grooves, and $L_{tri} = 3150$/m and another with 16 axial grooves, 56 circumferential grooves, and $L_{tri} = 2630$/m. A developmental view of the wick surface with $L_{tri} = 2630$/m is shown in Fig. 3. In addition, a classical wick with only 16 axial grooves and 1-mm width of the groove was also tested.

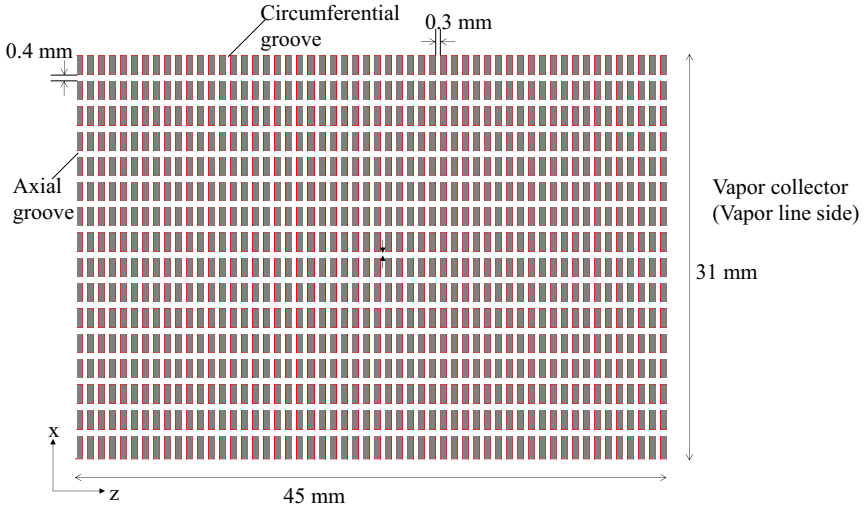

Fig. 3. Developmental view of the groove shape and the three-phase contact line (TPCL) at the contact surface between the wick and the case. There are 16 axial grooves and 56 circumferential ones. The 2630/m TPCL is shown in red. (For interpretation of the references to color in this figure legend, the reader is referred to the web version of this article.)

3. Results and discussion

The calculation conditions were as follows. The heat flux applied to the casing was 2 W/cm^2. The wick material was PTFE with a bulk thermal conductivity of 0.25 W/m·K, and the thermal conductivity of the stainless steel casing was 16 W/m·K. The working fluid was ethanol. The fluid properties were calculated using the Reference Fluid Thermodynamic and Transport Properties (REFPROP) program [29]. The detailed experimental apparatus is presented in [13].

Note that ΔP_{gr} was calculated using Eq. (10) and is shown in Fig. 4. It can be seen in Fig. 4 that pressure loss increases with the TPCL length. When a wick with a long TPCL is used, vapor velocity in the axial grooves is faster because there are fewer such grooves (Fig. 2). In addition, the pressure loss in the circumferential grooves is larger because the neighboring axial grooves are farther apart (see the arrows at the center of Fig. 3). The two abovementioned observations are the reason why pressure loss increases with the TPCL length. The pressure loss of evaporation (29 Pa) is independent of the TPCL length and is a negligible effect.

A comparison between the value of the evaporator heat-transfer coefficient obtained using Eq. (9) and that obtained through the experiments is presented in Fig. 5. In the calculation, two values of h_{tri} were used (see Table 2). One was calculated from the simulation results of [27], and the other was obtained by fitting the calculated results to the experimental ones. In both the experiment and the proposed model, the heat-transfer coefficient reached a local maximum in terms of the TPCL length, thus validating the model. It was found that the peak shifts to the left with larger pressure loss in the groove; the results obtained using the proposed model are in good agreement with the experimental ones. To more precisely calculate the pressure loss in both grooves, a 3D thermofluid simulation would be needed.

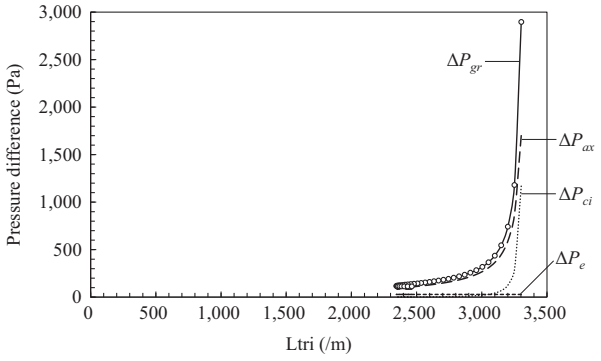

Fig. 4. Groove pressure loss as a function of the TPCL length.

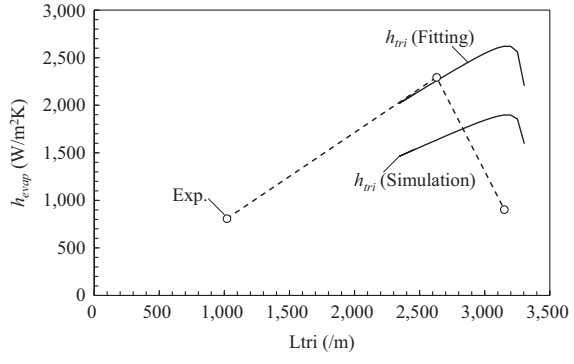

Fig. 5. Evaporator heat-transfer coefficient as a function of the TPCL length: h_{tri} = 0.87 is obtained from the calculated results fitted to experimental ones, and h_{tri} = 0.63 is obtained from calculated results using a three-dimensional evaporator simulation [27].

The reason for the difference between the values of h_{tri} obtained via the experiment and simulation could be that the latter does not take into account the meniscus at the TPCL in the evaporator heat-transport process. The effect of this meniscus could be significant, especially at low heat flux. The applied heat can flow directly to the groove via the meniscus. If this heat-flow path is considered in the simulation, the evaporator heat-transfer coefficient increases and the model results show good agreement with experimental ones. A heat-transport model that considers the meniscus at the TPCL is needed to evaluate h_{tri} more precisely. As the TPCL length increases, the contribution of the heat transport per unit TPCL length decreases because of dispersal of the heat flux. For the abovementioned reason, h_{tri} may decrease with TPCL length. This is also the cause of the difference in the values calculated via the experiment and simulation.

The experiments yielded curves with local maxima even at heat fluxes of 0.63 and 1.3 W/cm^2. For the 2630/m wick, the maximum heat flux was 3.4 W/cm^2 and the heat-transfer coefficient was 2400 W/m^{2}K.

To investigate the effect of the combination of materials in the evaporator, LHP simulation [27] values of h_{tri} were calculated for the following wick/fluid combinations: PTFE/ammonia, SS/ammonia, and copper/water. The results are listed in Table 3. Only PTFE/ammonia was in an unsaturated state; the other two were saturated. Note that h_{tri} increased with the wick's thermal conductivity. Comparing ammonia to ethanol (Table 2), the h_{tri} value is clearly higher for ammonia. This could be because of changes in the interfacial heat-transfer coefficient at the boundaries of the evaporation surface.

The evaporation rate at the wick/groove interface was calculated using the interfacial heat-transfer coefficient h_i [30]. Table 4 lists the value of h_i for each working fluid; ammonia showed the highest value.

The TPCL lengths and h_{tri} values calculated from the literature are listed in Table 5; h_{tri} was calculated using the following equation:

$$h_{tri} = \frac{h_{evap}}{L_{tri}} \tag{13}$$

Note that it is the area of the heat load that is used in the calculation of h_{evap} in this study and not the wick-case contact-surface area. In certain references, h_{evap} had to be recalculated if the original calculation was made using the wick-case contact area. Refs. [16], [21], and [23] created structures whose TPCLs were longer than that of the wick used in this study. A high groove density and a small groove width result in a long TPCL. Refs. [16] and [21] used TPCLs with the same length; however, the wick groove dimensions (height × width) used by Refs. [16] and [21] were 0.2 × 0.2 mm and 0.1 × 0.1 mm. respectively. Because the grooves used by

Table 2
Contribution of heat transport at the TPCL (h_{tri}) by PTFE wick, ethanol LHP, and 2 W/cm^2 of applied heat flux.

	Fitting to experiment	Simulation [27]
h_{tri} (W/m·K)	0.87	0.63

Table 3
Values of h_{tri} calculated via 3D simulation [27] for different wick/fluid materials and 2 W/cm^2 of applied heat flux.

	PTFE/ammonia	SS/ammonia	Copper/water
h_{tri} (W/m·K)	2.4 (2Φ)	3.7	8.8

Table 4
Interfacial heat-transfer coefficient (h_i) at 30 °C (obtained from REFPROP [29]).

	Acetone	Ammonia	Ethanol	Methanol	R134a	Water
h_i (W/m^{2}K)	30,800	784,000	17,900	35,200	185,000	12,300

Table 5
TPCL length (L_{tri}) and h_{tri} values obtained from the literature.

Reference	L_{tri} (/m)	Case material	Wick material	Working fluid	h_{tri} (W/m·K)
Nishikawara et al. [13]	510	SS 316	PTFE	Ethanol	1.7–2.7
		SS 316	PTFE	Acetone	1.4–2.5
		SS 316	PTFE	R134a	1.7–6.6
Riehl et al. [16]	5,000	SS 316	UHMW	Acetone	0.25–0.50
Kiseev et al. [17]	1,100	Copper	Nickel	Water	1.8–11
			Nickel	Acetone	1.8–7.2
			Titanium	Water	1.8–18
			Titanium	Acetone	1.8–14
Hodot et al. [19]	1,100	Copper	Nickel	Methanol	7.9
Yakomaskin et al. [21]	5,000	Copper	Glass fiber	Water	1.2–2.5
Wu et al. [22]	710	SS	Nickel	Ammonia	62
Uchida [23]	6,600	Copper	PTFE	Ethanol	0.45–0.39
This work	2,630	SS 316	PTFE	Ethanol	0.51–0.98

Ref. [21] were machined via the DCM and the case fin was sharp, it is assumed that contact between the case and the wick was at a point. Although the width of the groove used by Ref. [23] was 0.5 mm, the value of L_{tri} in that case is the largest of all because the grooves were formed along with depth direction of the wick. Results with large values of L_{tri} show low values of h_{tri}. As mentioned above, the reason for this is that the heat transport per unit TPCL length is dispersed. The h_{tri} value obtained by Ref. [22] using ammonia as the working fluid is the highest of all. This makes it clear that the h_i values listed in Table 4 have a significant effect on the h_{tri} ones. Given that the wettability of the TPCL is important, not only the wettability of the wick but also that of the case material can be important for highly efficient heat transfer.

4. Conclusions

In this paper, a model for the heat-transfer coefficient of an evaporator was proposed by just using the TPCL length of the case, a wick, and grooves to optimize wick shape in the capillary evaporator of LHPs and CPLs. The features of the proposed model were designed to allow the following two behaviors to be considered. The heat-transfer coefficient increased initially with TPCL length but then decreased when the TPCL length became too long because of a large distribution of saturation temperature caused by a large pressure loss in the grooves. The proposed model was validated experimentally. The experimental and model results show that the heat-transfer coefficient reached a local maximum in terms of the TPCL length. Therefore, it was concluded that the wick shape could be optimized by just using TPCL length. To assess the effects of the evaporator case, wick materials, and the working fluid, values of the heat transport at TPCL (h_{tri}) were calculated from the literature. These results indicate that the interfacial heat-transfer coefficient has an impact on the heat transport at the TPCL. In order to obtain more accurate results, a 3D simulation of vapor in the grooves and a model that considers meniscus effects at the TPCL are required.

Acknowledgments

This research was partly supported by JSPS KAKENHI Grant Number 15H06287 and by JST, PRESTO. The authors would like to thank Enago (www.enago.jp) for the English language review.

References

[1] A. Okamoto, R. Hatakenaka, T. Miyakita, H. Sugita, Development of 100W-class Loop Heat Pipes for Space Use and On-orbit Experiment Test Plan, in: Joint 18th IHPC and 12th IHPS, 2015: pp. 339–343.
[2] C. Figus, L. Dandaleix, J. Hill, L. Barremaecker, A Novel "Multi-Stages" Loop Heat Pipe for Cooling Multiple Heat Sources, in: Joint 18th IHPC and 12th IHPS, 2016: pp. 27–32.
[3] V. Dupont, S. Vanoost, L. Barremaecker, Railways qualification tests of capillary pumped loop on a train, in: 17th International Heat Pipe Conference, 2013.
[4] B.J. Huang, P.C. Hsu, R.J. Tsai, M.M. Hussain, A thermoelectric generator using loop heat pipe and design match for maximum-power generation, Appl. Therm. Eng. 91 (2015) 1082–1091, http://dx.doi.org/10.1016/j.applthermaleng.2015.08.059.
[5] B. Huang, Y.H. Chuan, P.E. Yang, Low-cost manufacturing of loop heat pipe for commercial applications, in: Joint 18th IHPC and 12th IHPS, 2016: pp. 599–602.
[6] Z.R. Lin, W.Z. Lin, L.W. Zhang, S.F. Wang, An experimental study on applying miniature loop heat pipes for laptop PC cooling, Semiconductor Thermal Measurement and Management Symposium (SEMI-THERM), 2013 29th Annual IEEE. (2013) 154–158. http://dx.doi.org/10.1109/SEMI-THERM.2013.6526821.
[7] J. Li, F. Lin, D. Wang, W. Tian, A loop-heat-pipe heat sink with parallel condensers for high-power integrated LED chips, Appl. Therm. Eng. 56 (2013) 18–26, http://dx.doi.org/10.1016/j.applthermaleng.2013.03.016.
[8] R. Singh, A. Akbarzadeh, M. Mochizuki, Effect of wick characteristics on the thermal performance of the miniature loop heat pipe, J. Heat Transfer 131 (2009) 082601, http://dx.doi.org/10.1115/1.3109994.
[9] S.C. Wu, D. Wang, Y.M. Chen, Investigating the effect of double-layer wick thickness ratio on heat transfer performance of loop heat pipe, Int. J. Therm. Sci. 86 (2014) 292–298, http://dx.doi.org/10.1016/j.ijthermalsci.2014.07.014.
[10] L. Mottet, M. Prat, Numerical simulation of heat and mass transfer in bidispersed capillary structures: application to the evaporator of a loop heat pipe, Appl. Therm. Eng. 102 (2016) 770–784, http://dx.doi.org/10.1016/j.applthermaleng.2016.03.143.
[11] V.M. Kiseev, V.V. Vlassov, I. Muraoka, Optimization of capillary structures for inverted meniscus evaporators of loop heat pipes and heat switches, Int. J. Heat Mass Transf. 53 (2010) 2143–2148, http://dx.doi.org/10.1016/j.ijheatmasstransfer.2009.12.032.
[12] V.V. Maziuk, V.V. Doctarau, A.A. Rak, Miniature loop heat pipes with noninverted meniscus concept and treatment, Int. J. Low-Carbon Technol. 1 (2006) 228–235, http://dx.doi.org/10.1093/ijlct/1.3.228.
[13] M. Nishikawara, H. Nagano, Parametric experiments on a miniature loop heat pipe with PTFE wicks, Int. J. Therm. Sci. 85 (2014) 29–39, http://dx.doi.org/10.1016/j.ijthermalsci.2014.05.016.
[14] M. Nishikawara, H. Nagano, Numerical simulation of capillary evaporator with microgap in a loop heat pipe, Int. J. Therm. Sci. 102 (2016) 39–46, http://dx.doi.org/10.1016/j.ijthermalsci.2015.11.008.
[15] M.T. North, D.B. Sarraf, J.H. Rosenfeld, Y.F. Maidanik, S. Vershinin, High heat flux loop heat pipes, AIP Conf. Proc. 387 (1997) 371–376.
[16] R.R. Riehl, N. Santos, N. dos Santos, Loop heat pipe performance enhancement using primary wick with circumferential grooves, Appl. Therm. Eng. 28 (2008) 1745–1755, http://dx.doi.org/10.1016/j.applthermaleng.2007.11.005.
[17] V.M. Kiseev, V.V. Vlassov, I. Muraoka, Experimental optimization of capillary structures for loop heat pipes and heat switches, Appl. Therm. Eng. 30 (2010) 1312–1319, http://dx.doi.org/10.1016/j.applthermaleng.2010.02.010.

[18] M. Kuroi, H. Nagano, The influence of groove shape on loop heat pipe performance, Heat Pipe Sci. Technol., Int. J. 3 (2012) 203–222.
[19] R. Hodot, V. Sartre, F. Lefevre, C. Sarno, 3D modeling and optimization of a loop heat pipe evaporator, in: 17th International Heat Pipe Conference. (2013) 1–6.
[20] A.A. Yakomaskin, V.N. Afanasiev, N.N. Zubkov, D.N. Morskoy, Investigation of heat transfer in evaporator of microchannel loop heat pipe, J. Heat Transfer 135 (2013) 101006, http://dx.doi.org/10.1115/1.4024502.
[21] A.A. Yakomaskin, Prototype of thin loop heat pipe with glass fiber wick for compact electronics cooling, in: Joint 18th IHPC and 12th IHPS, 2016: pp. 636–641.
[22] S.C. Wu, D. Wang, J.H. Gao, Z.Y. Huang, Y.M. Chen, Effect of the number of grooves on a wick's surface on the heat transfer performance of loop heat pipe, Appl. Therm. Eng. 71 (2014) 371–377, http://dx.doi.org/10.1016/j.applthermaleng.2014.06.042.
[23] H. Uchida, Thermal performance of a loop heat pipe containing an evaporator with a pin array conduction structure for electronic devices, Therm. Sci. Eng. 22 (2014) 85–95, http://dx.doi.org/10.11368/tse.22.85 (in Japanese).
[24] J. Li, G.P. Peterson, 3D heat transfer analysis in a loop heat pipe evaporator with a fully saturated wick, Int. J. Heat Mass Transf. 54 (2011) 564–574, http://dx.doi.org/10.1016/j.ijheatmasstransfer.2010.09.014.
[25] X. Zhang, X. Li, S. Wang, Three-dimensional simulation on heat transfer in the flat evaporator of miniature loop heat pipe, Int. J. Therm. Sci. 54 (2012) 188–198, http://dx.doi.org/10.1016/j.ijthermalsci.2011.12.002.
[26] M. Nishikawara, H. Nagano, L. Mottet, M. Prat, Formation of unsaturated regions in the porous wick of a capillary evaporator, Int. J. Heat Mass Transf. 89 (2015) 588–595.
[27] M. Nishikawara, H. Nagano, and M. Prat, A numerical study on heat transfer characteristics of a loop heat pipe evaporator using three-dimensional pore network model, in: Proc. of the Joint 18th International Heat Pipe Conference and 12th International Heat Pipe Symposium, No. 140044, Jeju, Jun., 2016.
[28] K. Oshima, T. Matsushita, M. Murakami, Heat Pipe Engineering, Asakura Publishing Co., Ltd., 1979.
[29] E.W. Lemmon, M.L. Huber, M.O. McLinden, NIST Standard Reference Database 23: Reference Fluid Thermodynamic and Transport Properties-REFPROP, Version 9.1, National Institute of Standards and Technology, Standard Reference Data Program, Gaithersburg, 2013.
[30] V.P. Carey, Liquid–Vapor Phase-Change Phenomena, first ed., Taylor & Francis, 1992.